

Imaging Field-Driven Melting of a Molecular Solid at the Atomic Scale

Franklin Liou, Hsin-Zon Tsai, Zachary A. H. Goodwin, Andrew S. Aikawa, Ethan Ha, Michael Hu, Yiming Yang, Kenji Watanabe, Takashi Taniguchi, Alex Zettl, Johannes Lischner, and Michael F. Crommie*

Solid–liquid phase transitions are basic physical processes, but atomically resolved microscopy has yet to capture their full dynamics. A new technique is developed for controlling the melting and freezing of self-assembled molecular structures on a graphene field-effect transistor (FET) that allows phase-transition behavior to be imaged using atomically resolved scanning tunneling microscopy. This is achieved by applying electric fields to 2,3,5,6-tetrafluoro-7,7,8,8-tetracyanoquinodimethane-decorated FETs to induce reversible transitions between molecular solid and liquid phases at the FET surface. Nonequilibrium melting dynamics are visualized by rapidly heating the graphene substrate with an electrical current and imaging the resulting evolution toward new 2D equilibrium states. An analytical model is developed that explains observed mixed-state phases based on spectroscopic measurement of solid and liquid molecular energy levels. The observed nonequilibrium melting dynamics are consistent with Monte Carlo simulations.

the single-particle scale. Great progress has been made at controlling structural, electronic, and magnetic phase transitions in different materials by varying macroscopic parameters such as strain,^[1–3] density,^[4,5] and electromagnetic fields,^[6–9] but imaging the atomic-scale dynamics of such transitions has proved difficult. The reason for this is the difficulty of combining atomic-scale microscopy with the high bandwidth required to capture fast dynamics. Here we describe a different approach for exploring dynamical processes that involve rapidly quenching the thermally-induced kinetics of 2D phase transitions and imaging their evolution toward equilibrium frame-by-frame using atomically resolved scanning tunneling microscopy (STM).

We have used this technique to image the electrostatically driven solid–liquid phase transition of 2,3,5,6-tetrafluoro-7,7,8,8-

tetracyanoquinodimethane (F_4 TCNQ) molecules at the surface of a graphene field-effect transistor (FET) held at cryogenic temperature in ultrahigh vacuum. Voltages applied to the back gate of such a device induce reversible freezing and melting of molecular

1. Introduction

Phase transitions reflect the collective behavior of large numbers of particles but originate from rapid reconfigurations at

F. Liou, H.-Z. Tsai, A. S. Aikawa, E. Ha, M. Hu, Y. Yang, A. Zettl, M. F. Crommie

Department of Physics
University of California at Berkeley
Berkeley, CA 94720, USA

E-mail: azettl@berkeley.edu; crommie@berkeley.edu

F. Liou, H.-Z. Tsai, A. S. Aikawa, A. Zettl, M. F. Crommie
Materials Sciences Division
Lawrence Berkeley National Laboratory
Berkeley, CA 94720, USA

F. Liou, A. Zettl, M. F. Crommie
Kavli Energy NanoSciences Institute at the University of California at Berkeley
Berkeley, CA 94720, USA


Z. A. H. Goodwin, J. Lischner
Department of Materials
Imperial College London
Prince Consort Rd, London SW7 2BB, UK
E-mail: j.lischner@imperial.ac.uk

Z. A. H. Goodwin
National Graphene Institute
University of Manchester
Booth St. E. Manchester M13 9PL, Manchester UK

Z. A. H. Goodwin
School of Physics and Astronomy
University of Manchester
Oxford Road, Manchester M13 9PL, UK

K. Watanabe
Research Center for Electronic and Optical Materials
National Institute for Materials Science
1-1 Namiki, Tsukuba 305-0044, Japan

T. Taniguchi
Research Center for Materials Nanoarchitectonics
National Institute for Materials Science
1-1 Namiki, Tsukuba 305-0044, Japan

 The ORCID identification number(s) for the author(s) of this article can be found under <https://doi.org/10.1002/adma.202300542>

DOI: 10.1002/adma.202300542

structures at the surface, but the evolution of these structures toward new equilibrium states is quenched by the device's low temperature ($T \approx 4$ K). Equilibration can only be achieved by passing current through the graphene substrate, thereby transiently raising the temperature and speeding the molecular kinetics (i.e., the diffusive motion). Rapid cooling after the current is stopped allows "snapshots" of the surface molecular configuration to be taken without the need for ultrafast imaging techniques. Stop-motion movies of field-induced molecular phase transitions can be made this way that have atomic spatial resolution and a time resolution set by the electronic and thermal relaxation time constants of the device.^[10] This has allowed us to resolve the melting and freezing processes of F_4 TCNQ molecules at the single-molecule level in both liquid and solid phases, something not possible via other microscopy techniques^[11–13] due to the non-crystallinity and fast dynamics of molecular liquids.^[11,12]

Scanning tunneling spectroscopy (STS) measurements reveal that a solid phase of F_4 TCNQ is favored when the graphene Fermi level (E_F) is lowered to a point where the molecules become charge-neutral. Raising E_F sufficiently with a back-gate causes the solid F_4 TCNQ phase to melt into a liquid phase in a process where each molecule converted to the liquid phase accepts a single electron. The F_4 TCNQ liquid phase is thus populated by negative ions.^[14] We have developed a simple theoretical framework that explains the equilibrium energetics of this first-order solid–liquid phase transition as a function of gate voltage, and have performed Monte Carlo simulations that capture its nonequilibrium melting dynamics.

2. Results

Figure 1 shows the reversible melting/freezing of a partial monolayer of F_4 TCNQ on a graphene FET as it transitions through different equilibrium states in response to the applied back-gate voltage V_G . For $V_G = -30$ V (Figure 1a) the molecules all lie in a solid "chain" phase after flowing source–drain current $I_{SD} = 1$ mA through the device for 180 s (all STM images and spectroscopy are acquired only after setting I_{SD} to zero to quench molecular motion by reestablishing the device base temperature of $T = 4.5$ K). Figure 1j shows close-up STM and AFM images of the F_4 TCNQ solid phase revealing two quasi-1D chain morphologies that we call "linear" and "zigzag" (more detailed structural characterization can be found in Figures S7 and S8, Supporting Information). The structure factor of the chain phase shows clear periodicity, thus indicating that it is a quasi-1D crystalline solid (see additional details in Section 8, Figure S7, Supporting Information).

Subsequent raising of the gate voltage to $V_G = 0$ V followed by application of "diffusive" conditions (i.e., by setting $I_{SD} = 1$ mA) for 180 s causes the molecular solid to partially melt. This can be seen in Figure 1b which shows isolated F_4 TCNQ molecules dotting the surface near the edge of the solid phase in the same area as Figure 1a (the isolated molecules belong to a 2D liquid phase as described below). This is an equilibrium configuration in the sense that the average concentrations of the liquid and solid phases have stopped changing with time under diffusive conditions. The images in Figure 1c,d show the equilibrium configurations of the same region after incrementally raising the gate voltage first to $V_G = 6$ V and then to $V_G = 30$ V under diffu-

sive conditions. For every step increase in V_G , the solid is seen to melt a little more until it is completely liquefied at $V_G = 30$ V. Figure 1e–h shows the same surface region as V_G is decreased back to -30 V under identical diffusive conditions. The liquid–solid phase transition is completely reversible (movies of the freezing/melting processes are shown in Movies S1 and S2, Supporting Information).

Justification for calling the phase containing isolated molecules (Figure 1d) a liquid comes from an analysis of the molecular radial distribution function, $g(r)$, and structure factor, $S(q)$. Figure 1k shows $g(r)$ extracted from a large-area image containing isolated molecules prepared under equilibrium conditions (see Section 1, Supporting Information for additional details). $g(r)$ shows evenly spaced peaks with a spacing of $a = 3.84$ nm, as expected for the shell structure of an isotropic liquid.^[15] The structure factor seen in the Figure 1k inset (for the same STM image) is also indicative of an isotropic liquid and shows no evidence of crystal or gas behavior.^[15]

Understanding the cause of the observed molecular phase transition requires understanding how charge transfers between molecules and graphene under different gating conditions. STS measurements were used to gain insight into this process by separately measuring the local electronic structure of the solid and liquid phases. **Figure 2a** shows dI/dV spectra measured on an F_4 TCNQ chain (solid phase) compared to an isolated F_4 TCNQ molecule (liquid phase) for $V_G = -60$ V (this is the hole-doped graphene regime as shown by the inset electronic structure diagram in Figure 2a). The bare graphene spectrum for this surface (taken 10 nm away from any molecules) is shown in the inset for reference. A dip in the bare graphene local density of states near $V = 0.34$ V marks the location of the graphene Dirac point (E_D), thus verifying that the graphene is in the hole-doped regime for this gate voltage. The gap-like feature at $V = 0$ (E_F) arises from a well-known phonon-assisted inelastic tunneling effect.^[16]

The blue curve in Figure 2a shows the dI/dV spectrum for a single, isolated F_4 TCNQ molecule (SM) in this hole-doped regime. The leading edge of the first peak marks the lowest unoccupied molecular orbital (LUMO) energy as discussed in previous work^[14,17] ($E_L^{SM} = 0.2$ eV and is marked by a dashed blue line), while the second peak ($V_b \approx 0.4$ V) is a phonon satellite arising from intramolecular vibrations.^[17] The F_4 TCNQ LUMO level is unoccupied for this value of V_G . The second curve (red) shows the dI/dV spectrum measured with the STM tip held over the end molecule of an F_4 TCNQ solid chain (the chain end (CE) as shown in Figure 1j). The CE spectrum is nearly identical to the single molecule spectrum except that E_L is shifted up by 0.06 eV. The third curve (orange) shows the spectrum for a molecule in the middle of a chain (CM) (as shown in Figure 1j). Here E_L is pushed up even further by an additional 0.05 eV. The overall energy-level structure is schematically represented by the inset sketch which shows the energy level alignment of the SM LUMO, the CE LUMO, and the CM LUMO relative to E_D and E_F (the experimental energy levels of the zigzag and linear chains are identical, as shown in Figure S9, Supporting Information).

This energy-level structure has important consequences for F_4 TCNQ/graphene solid–liquid phase transitions. For example, suppose that V_G was first set to $V_G = -60$ V (the case shown

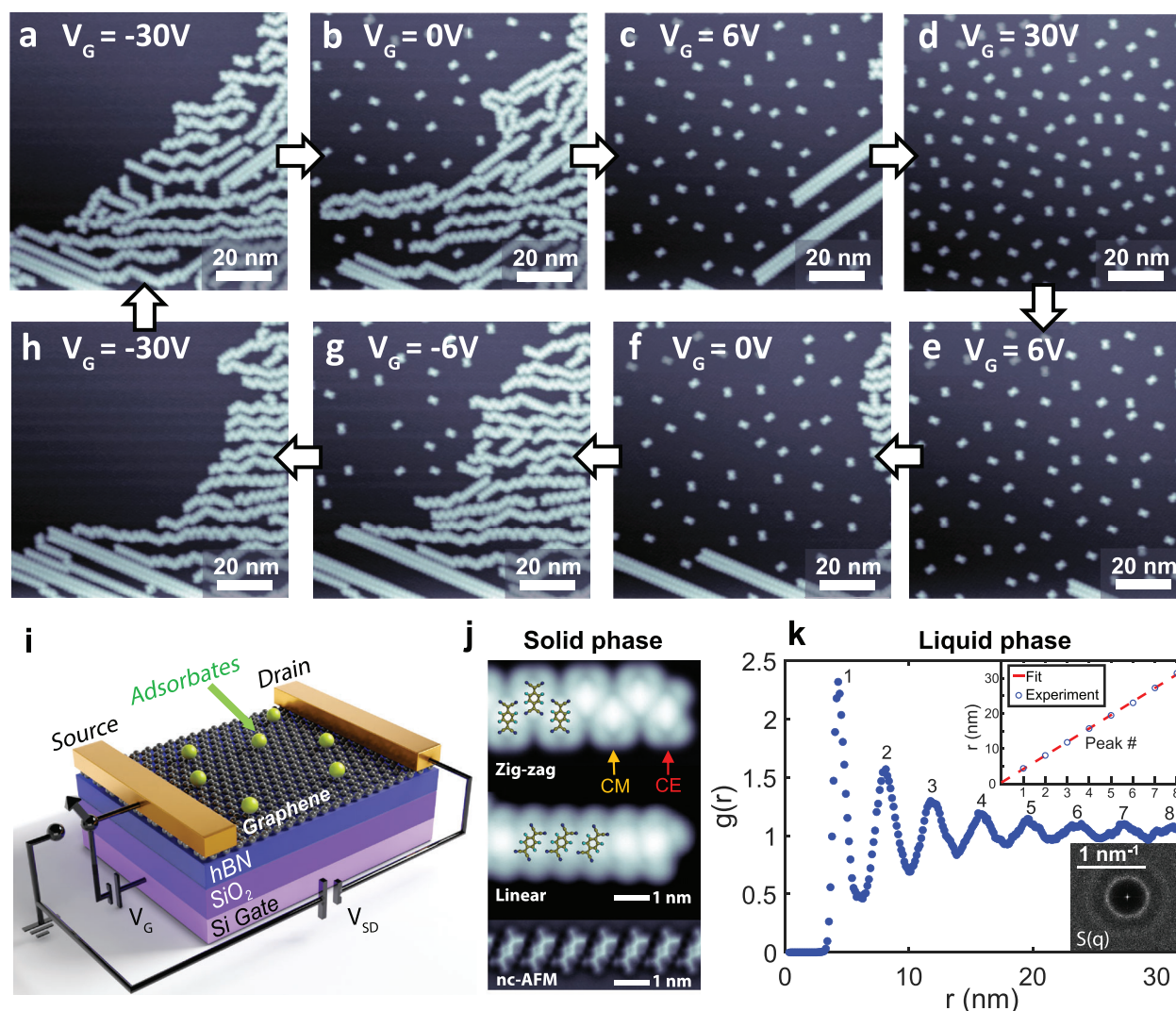


Figure 1. Gate-tunable solid–liquid molecular phase transition. a–d) STM images show the melting of self-assembled chains of F_4TCNQ molecules (solid phase) into isolated molecules (liquid phase) as V_G is increased through -30 V (a), 0 V (b), 6 V (c), 30 V (d). e–h) The reverse phase transition (liquid to solid) is observed at the same spot on the surface with molecules coalescing from the liquid phase into self-assembled chains as V_G is decreased through 6 V (e), 0 V (f), -6 V (g), -30 V (h). i) Schematic of the experimental setup shows F_4TCNQ molecules adsorbed onto the surface of a graphene FET device. j) Closeup STM images of the solid molecular chain phase (with structural overlays) show two observed geometries (linear and zig-zag), both having a center-to-center molecular distance of 8.5 Å. A bond-resolved nc-AFM image in the bottom row (obtained with a CO tip^[21]) reveals the linear geometry in greater detail. k) The radial distribution function $g(r)$ of molecular positions in the liquid phase shows shell-like structure having an average shell spacing of 3.84 nm (the corresponding STM image can be seen in Figure S1b, Supporting Information). The corresponding structure factor $S(q)$ shown in the inset indicates that the liquid is isotropic. STM images were obtained at $T = 4.5$ K.

in Figure 2a) and then slowly increased under diffusive conditions. This would cause E_F to slide to the right and eventually intersect E_L^{SM} . The first molecules to fill with charge due to the increasing V_G would thus be isolated F_4TCNQ molecules. As shown previously,^[14] under these conditions E_F becomes pinned close to E_L^{SM} and so never reaches the chain orbitals (E_L^{CE} or E_L^{CM}) which therefore remain charge-neutral (i.e., unoccupied) for a wide range of V_G values. Increasing V_G while E_F is pinned in this way causes molecules to melt from the neutral solid and to fill with charge, thereby increasing the molecular density of the charged liquid phase (separation between the isolated molecules is explained by Coulomb repulsion).

A useful thermodynamic variable to characterize this process is the total charge density in the molecule-decorated graphene system, $-\Delta Q$ (this counts the excess density of electrons). When the molecular chains begin to melt in response to increased V_G , $-\Delta Q$ exhibits a discontinuous jump when plotted as a function of E_F as shown in Figure 2b. Here $-\Delta Q$ is obtained from the relationship $-\Delta Q = CV_G$ where C is the capacitance per area between the graphene and the gate electrode. E_F and E_D are measured as a function of V_G from STM spectroscopy (by fitting dI/dV spectra such as that shown in the inset to Figure 2a), and the discontinuity in $-\Delta Q$ is observed to occur at $E_F - E_D \approx -0.125$ eV. For $E_F - E_D < -0.125$ eV the molecules

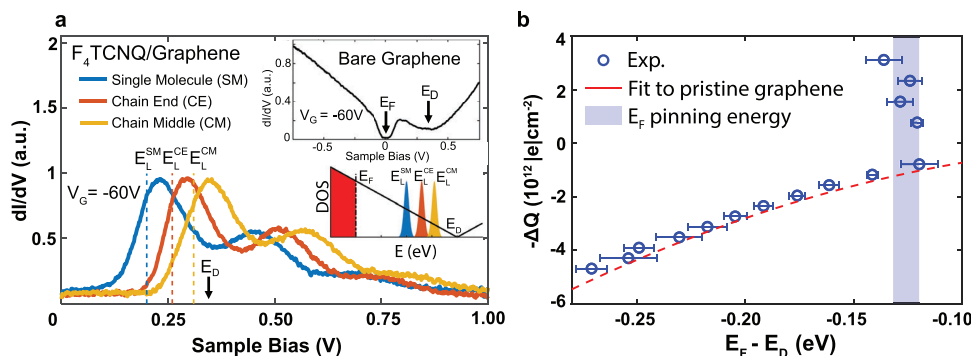


Figure 2. Electronic energy level alignment and charge accumulation under electrostatic gating. a) dI/dV spectra taken at $V_G = -60$ V for F_4 TCNQ molecules at a chain middle (CM), a chain end (CE), and for single, isolated molecules (SM) (images shown in Figure 1). The inset plot shows the dI/dV spectrum measured on bare graphene for $V_G = -60$ V. The inset sketch shows the relative energy alignments of the CM LUMO state, the CE LUMO state, the SM LUMO state, the Fermi energy (E_F), and the Dirac point (E_D). b) Total charge density accumulated in the molecule/graphene surface (measured capacitively and plotted in terms of electron density) as a function of $E_F - E_D$ (as determined by STS). A discontinuity is seen at $E_F - E_D = -0.125$ eV. STS spectra obtained at $T = 4.5$ K.

are in the charge-neutral chain phase where increases in $-\Delta Q$ reflect the filling of the graphene Dirac band (thus leading to a well-known parabolic dependence of $-\Delta Q$ on E_F in graphene).^[18] When E_F reaches the critical value of $E_F - E_D = -0.125$ eV, however, charge begins to flow into the F_4 TCNQ LUMO states as the chain phase melts to accommodate added charge. The molecules have a high quantum capacitance at this energy and so device charge accumulates rapidly with increasing E_F , thus resulting in discontinuous behavior as shown in Figure 2b. While the discontinuity in $-\Delta Q$ reflects the electronic part of the phase transition, concurrent imaging of molecular chain dissociation (i.e., molecular melting) shows that this electronic change accompanies the structural phase transition. The E_F dependence of $-\Delta Q$ in Figure 2b is reminiscent of the temperature dependence of transferred heat in a standard temperature-driven solid–liquid melting transition (such as ice to water), where latent heat must be provided to increase entropy as the solid converts to a liquid. Here E_F is analogous to temperature and the number of excess electrons ($-\Delta Q$) is analogous to entropy, so one can think of “latent charge” as being necessary to induce 2D molecular melting in our devices (see Section 10, Supporting Information for more detailed discussions of this analogy). Similar thermodynamic models of electrostatically driven phase transitions have been utilized to explain solid–solid phase transitions in 2D materials.^[19]

These insights enable us to develop a theoretical model for quantitatively understanding the microscopic energetics of the F_4 TCNQ/graphene solid–liquid phase transition. We first note that the F_4 TCNQ molecules and graphene both exchange electrons with the gate which acts as a reservoir. The thermodynamics of such an open system for electrons is described by the grand potential (see Section 10, Supporting Information for a more detailed discussion). Under our low-temperature experimental conditions (which rise to ≈ 25 K when $I_{SD} \neq 0$) the entropy contribution TS to the grand potential is expected to be small, and so we model the grand potential as follows:

$$\Phi = U - E_F N_e \quad (1)$$

Here U is the total energy of the graphene plus molecules and N_e is the total number of electrons in the graphene/molecule system relative to a reference state. The reference here is the configuration where all electrons occupy graphene band states with energy $E < E_L^{SM}$ and the molecules are uncharged. Since the LUMO energy of the chains is higher than that of isolated molecules, we ignore the possibility of the chains becoming charged and assume that electrons occupy either single-molecule LUMO states or graphene Dirac band states. The graphene contribution to the total energy relative to the reference state is denoted by $U_g(E_F) = \int_{E_L}^{E_F} \epsilon g(\epsilon) d\epsilon$, where $g(\epsilon)$ is found from the well-known linear band model^[20] to be $g(\epsilon) = 2A(E_D - \epsilon)/\pi\hbar^2 v_F^2$ (here E_D is the Dirac point energy, A is the area of graphene, and v_F is the Fermi velocity). If we assume that our system has a total of N molecules that are all in the neutral chain phase, then the molecular energy can be approximated as $U_s(N) \approx -\alpha N$ where $-\alpha$ corresponds to the energy per bond between adjacent molecules. We denote the number of electrons in this pure solid phase as $N_{e,s}$, in which case the grand potential is

$$\Phi_s = U_s(N) + U_g(E_F) - E_F N_{e,s} \quad (2)$$

On the other hand, if the N molecules are all in the charged liquid phase then the molecules are each charged by one electron in the LUMO and the molecular contribution to the total energy becomes $U_l(N) = E_L N$ (for simplicity we have dropped the superscript “SM” from E_L). We denote the number of electrons in this pure liquid phase as $N_{e,l}$, in which case the grand potential is

$$\Phi_l = U_l(N) + U_g(E_F) - E_F N_{e,l} \quad (3)$$

The critical Fermi level (E_F^c) at which the phase transition occurs is determined by setting $\Phi_s = \Phi_l$. At this Fermi level $N_{e,l} - N_{e,s} = N$ since N electrons are needed to charge the molecules, thereby yielding $E_F^c = E_L + \alpha$. For $E_F < E_F^c$ all of the electrons reside in graphene band states and all of the molecules are condensed into solid chains due to the energy gain of bond formation. For $E_F > E_F^c$, on the other hand, all of the molecules are in the charged liquid state. The transition from the solid phase to the liquid phase

does not occur when $E_F = E_L$ because melting the chains requires extra energy to break the bond between a chain end molecule and its neighbor (i.e., the latent heat of melting). The process of adding a charged, isolated molecule to the liquid phase only becomes energetically favorable when the Fermi level reaches a value equal to E_L plus the energy required to break one bond (α). This insight allows us to, in principle, experimentally obtain α by comparing the measured value of E_F^c at which the phase transition occurs (which is marked by Fermi level pinning) to spectroscopic measurements of E_L . Experimentally we observe E_F^c to be 120 ± 20 meV below the Dirac point energy and E_L to be 140 ± 5 meV below the Dirac point (E_L was determined previously^[14]). The difference between these quantities is on the order of our experimental uncertainty, and so we are not yet able to extract an accurate value of α from our data. We are, however, able to place an upper limit on α : $\alpha \leq 40$ meV (which is consistent with a DFT-based estimate of α , see Section 5b, Supporting Information).

While the grand potential is continuous at the phase transition, its first derivative with respect to E_F is not. From Equations (2) and (3) we see that $\frac{\partial \Phi_l}{\partial E_F}$ and $\frac{\partial \Phi_s}{\partial E_F}$ differ by N at $E_F = E_F^c$, confirming that this is a first-order phase transition. In a heat-driven first-order phase transition, such as the transformation of ice to liquid water, latent heat is required to convert the phases at the transition temperature. Our phase transition, however, is not heat-driven but is rather driven by electrostatic gating. There is thus a latent charge of N electrons required for complete conversion of N molecules in the solid phase to the liquid phase rather than a latent heat. This is consistent with the experimental discontinuity in $-\Delta Q$ seen in Figure 2b which reflects the charge transferred to melt F_4TCNQ while E_F is pinned at the critical value, analogous to how latent heat is transferred to melt a solid while the temperature is pinned at the melting point in a heat-driven solid–liquid phase transition.

The preceding discussion is relevant for equilibrium conditions of the pure liquid phase ($E_F > E_F^c$) vs the pure solid phase ($E_F < E_F^c$), but we are also able to characterize the nonequilibrium solid–liquid (mixed phase) coexistence regime (i.e., unstable excursions from $E_F = E_F^c$) where the proportion of molecules in the chain and liquid phases can be adjusted from one equilibrium state to another (Figure 3). Figure 3a shows a plot of the experimental liquid phase molecular density (N_l/A , where A is the graphene area) vs $V_G - V_0$ where $V_0 = -10$ V is the gate voltage at which isolated molecules first appear in STM images. The yellow dots in Figure 3a shows that the experimental equilibrium values for N_l/A exhibit a linear dependence on gate voltage. The magenta dots, on the other hand, show experimental nonequilibrium data obtained by changing V_G and I_{SD} in such a way that diffusive conditions do not last long enough for the system to fully equilibrate. Figure 3b–g shows a full cycle of the system (measured at a single location on the device) as it evolves from one equilibrium configuration to a different one (yellow dots) and then back again by transitioning through a series of intermediate nonequilibrium states (magenta dots).

To understand this experimental process, we start with Figure 3b which shows a patch of the surface that was initially in an equilibrium state at $V_G - V_0 = 60$ V. At this gate voltage a relatively high liquid phase density ($N_l/A = 4.1 \times 10^{12}$ molecules per cm^2) coexists with a much lower concentration of the solid phase. The gate voltage was then changed to $V_G - V_0 = 50$ V under non-

diffusive conditions (i.e., $I_{SD} = 0$) to set a new equilibrium target, but without allowing the system to evolve toward the new target (since the kinetics are quenched by keeping $I_{SD} = 0$). The resulting nonequilibrium configuration is denoted $t = 0$ (Figure 3b) and is visually identical to the equilibrium state at $V_G - V_0 = 60$ V. Figure 3c shows the same region after subjecting it to diffusive conditions (by setting $I_{SD} = 1.1$ mA) for $\Delta t = 50$ ms while holding the gate voltage constant at $V_G - V_0 = 50$ V. The solid phase density is seen to increase, but equilibrium is not yet established. Figure 3d shows the same region after allowing it to evolve for an additional 50 ms under diffusive conditions while maintaining $V_G - V_0 = 50$ V. The system is now in equilibrium with N_l/A reduced to 3.5×10^{12} molecules per cm^2 and the solid density correspondingly increased. Figure 3e–g show the same process in reverse as V_G is reset to the original value of $V_G - V_0 = 60$ V. The system is observed to evolve back to its original equilibrium configuration after passing through a nonequilibrium state (Figure 3f) regime.

The mixed-phase solid/liquid configurations observed in Figure 3 can be understood within our theoretical framework in a straightforward way. To do this we consider the total energy of a mixed phase state containing N_l molecules in the liquid phase and $N - N_l$ molecules in the chain phase given by

$$U(N_l, E_F) = U_l(N_l) + U_s(N - N_l) + U_g(E_F) \quad (4)$$

where U_l , U_s , U_g , and N are defined the same as for Equations (2) and (3). Here N is constant, and E_F is determined by V_G and N_l . Only N_l remains variable, and its value at equilibrium N_l^{eq} is obtained by minimizing Equation (4) with respect to N_l (see Section 4, Supporting Information for details). The resulting expression for N_l^{eq} per unit area is

$$\frac{N_l^{\text{eq}}}{A} = CV_G + \frac{|E_D - (E_L + \alpha)|^2}{\pi \hbar^2 v_F^2} \quad (5)$$

where A is the area of the graphene capacitor, E_L is the LUMO energy, E_D is the Dirac point energy, and v_F is the Fermi velocity near the Dirac point (1.1×10^6 m s^{-1}). This expression is similar to an expression derived in ref. [14] using a different approach, but the new expression differs in the last term of Equation (5) which arises due to the energy required to break a bond (α), a factor not considered in ref. [14]. Equation (5) is plotted in Figure 3a (white dashed line) and is seen to match the equilibrium data (yellow dots) quite well. The nonequilibrium behavior (magenta dots) can be explained by plotting U from Equation (4) as a color map depending on both V_G and N_l in Figure 3a. The low-energy region of $U(N_l, V_G)$ is seen to correspond precisely to the equilibrium density defined by Equation (5) (as expected). Excursions from equilibrium, as shown by the magenta dots, thus push the system to higher energy. The energy landscape of Figure 3a is consistent with the experimentally observed tendency of the system to relax back down in energy to the equilibrium configuration.

A more dramatic example of nonequilibrium behavior is shown in Figure 4 which exhibits the time evolution of a nonequilibrium melting process at a molecular solid–liquid interface. The STM image in Figure 4a shows the equilibrium configuration of this area at $V_G = -20$ V after sufficiently long

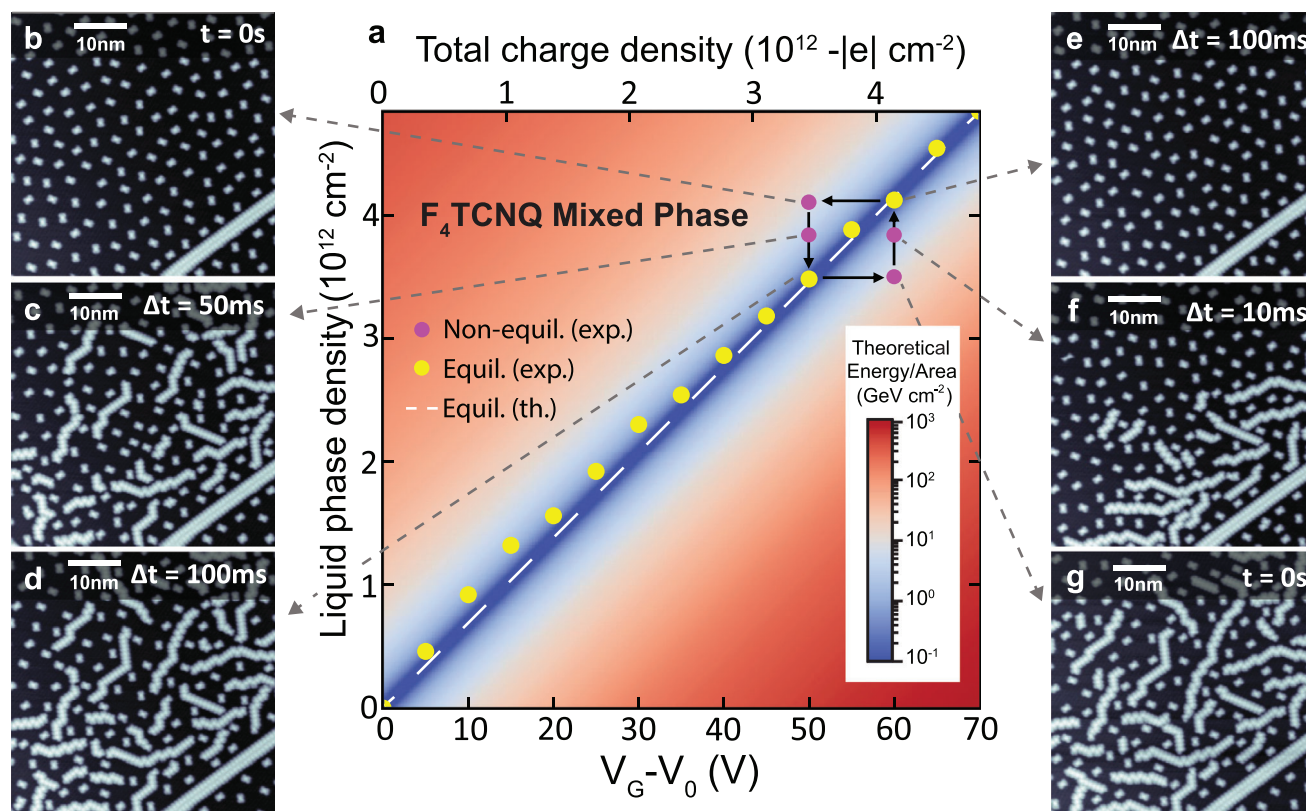


Figure 3. F_4 TCNQ chain freezing and melting under nonequilibrium conditions. a) Experimental values of the equilibrium liquid phase molecule density (N_l/A) are plotted as yellow dots and nonequilibrium values as magenta dots. The theoretical total energy of the equilibrium mixed phase of F_4 TCNQ/graphene is also shown (color scale) as a function of liquid phase surface density and gate voltage (V_0 is the gate voltage at which melting first begins). The minimum energy configuration corresponds to the dashed white line (obtained from Equation (5)). b) STM image of the nonequilibrium molecular state obtained by switching $V_G - V_0$ to 50 V starting from the equilibrium state at $V_G - V_0 = 60$ V and not allowing the system to evolve under diffusive conditions ($t = 0$). c) Molecular chains condense into a nonequilibrium state after allowing the system to evolve for 50 ms under diffusive conditions ($I_{SD} = 1.1$ mA, $V_G - V_0 = 50$ V). d) Molecular chain condensation advances to this equilibrium state after waiting an additional 50 ms under diffusive conditions ($I_{SD} = 1.15$ mA, $V_G - V_0 = 50$ V). e) STM image of the nonequilibrium state obtained by switching $V_G - V_0$ to 60 V and not allowing the system to evolve under diffusive conditions ($t = 0$). f) Molecular chains have partially melted in this nonequilibrium state obtained after allowing the system to evolve for 10 ms under diffusive conditions ($I_{SD} = 1.11$ mA, $V_G - V_0 = 60$ V). g) Molecular chains have melted even further in this equilibrium state obtained after waiting an additional 90 ms under diffusive conditions ($I_{SD} = 1.11$ mA, $V_G - V_0 = 60$ V), thus returning the molecular density to its initial configuration in (b). STM images were obtained at $T = 4.5$ K.

diffusive conditions. A region of high solid phase density can be seen in the upper left and zero liquid phase density throughout. The surface was then put into a nonequilibrium state by rapidly changing the gate voltage to $V_G = 60$ V (corresponding to a high liquid phase density equilibrium target). The system was then allowed to evolve under diffusive conditions for only $\Delta t = 500$ μ s before being quenched and imaged as shown in Figure 4b. This nonequilibrium snapshot shows a “wave” of liquid phase molecules emanating from the molecular solid like water from a melting glacier. The width of the liquid layer extends outward from the solid by ≈ 80 nm and exhibits an interparticle spacing that is mostly constant. Figure 4c shows the same area after allowing it to evolve under diffusive conditions for another 700 μ s. The layer of liquid now extends outward from the solid by more than 160 nm. A full video of this process can be found in Movie S3 (Supporting Information).

The theoretical framework discussed up to now is inadequate to model this type of nonequilibrium dynamics. To bet-

ter understand this melting process we have generalized our overall model to account for: i) multiple chains, ii) isolated uncharged molecules, and iii) screened Coulomb interactions between charged molecules. We have numerically simulated this more complete model using the Monte Carlo method (see Section 6, Supporting Information) to explain the dynamics shown in Figure 4a–c. An initial configuration was chosen with molecules arranged into chains (Figure 4d), similar to the F_4 TCNQ solids we observe experimentally. All model parameters were constrained by the experiment except for α (for which we only have an upper bound), but our results do not strongly depend on the precise value of α . A fixed number of electrons was added to the system at the start of the calculation to simulate the gating process, and the resulting liquid phase density and E_F value were subsequently determined. Overall, the simulation produced results quite similar to the experiment. For example, isolated molecules were observed to dissociate from chains after only a few Monte Carlo steps and to move toward empty graphene

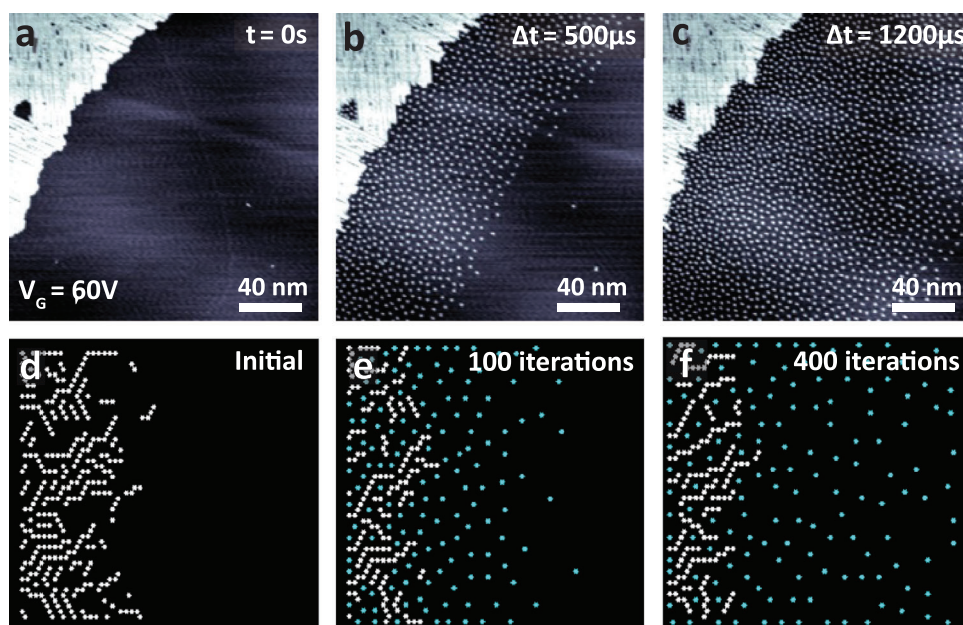


Figure 4. Nonequilibrium melting of the F_4TCNQ solid. a) STM image of an equilibrium F_4TCNQ solid formed under diffusive conditions on a graphene FET at $V_G = -20$ V. V_G was stepped up to $V_G = 60$ V before imaging, but the system was not allowed to evolve under diffusive conditions ($t = 0$). b) Same region of the surface after allowing it to evolve under diffusive conditions for $\Delta t = 500 \mu s$ ($I_{SD} = 1.3$ mA, $V_G = 60$ V). A “wave” of charged liquid phase molecules can be seen emanating from the solid interface. c) Same region after allowing the system to evolve for an additional $\Delta t = 700 \mu s$ under diffusive conditions ($I_{SD} = 1.3$ mA, $V_G = 60$ V). The flow of charged molecular liquid has extended even further from the condensed phase interface. d–f) Monte Carlo simulations of F_4TCNQ molecules disassociating from chains to model the behavior shown in (a–c). Molecules colored in blue are charged and can be seen flowing outward from the charge-neutral condensed phase interface. STM images were obtained at $T = 4.5$ K.

regions (Figure 4e,f), similar to the flow of molecules observed experimentally in Figure 4b,c.

3. Conclusion

We have observed a gate-tunable first-order solid–liquid phase transition for F_4TCNQ molecules adsorbed onto the surface of a graphene FET. We are able to control and image the relative abundances of liquid and solid phases for different equilibrium conditions and to directly visualize nonequilibrium processes with a single-molecule resolution for both the solid and liquid phases. We have developed an analytical model that explains the gate-dependent equilibrium properties of this system with the only unknown parameter being the energy of cohesion of the molecular solid. The techniques described here provide a new method for experimentally extracting this parameter, and our results put an experimental upper bound on it of 40 meV per molecule. Monte Carlo simulations show reasonable agreement with the highly nonequilibrium kinetics observed in our experiment. The phenomenology observed here should be generalizable to other adsorbate/surface systems that are similarly gate-tunable.

4. Experimental Section

Graphene Transistor Fabrication: Graphene/hexagonal boron nitride (hBN) FETs were fabricated on highly doped SiO_2/Si by mechanical exfoliation. Electrical source and drain contacts were fabricated by depositing 3 nm thickness of Cr and 10 nm thickness of Au through a stencil mask.

The doped silicon substrate was used as the back gate. After placing in UHV, the graphene surface was cleaned by high-temperature annealing in a vacuum at 400 °C for 12 h.

Molecule Deposition: F_4TCNQ molecules were loaded into a Knudsen cell evaporator and heated to 120 °C under ultrahigh-vacuum (UHV) conditions for deposition onto a graphene FET held at room temperature. Sub-monolayer molecular coverage was achieved by keeping the deposition time under 15 s.

STM/STS Measurements: STM/STS measurements were performed under UHV conditions at $T = 4.5$ K using a commercial Omicron LT STM with Pt/Ir tips. STM topography was obtained in constant-current mode. STM tips were calibrated on an Au(111) surface by measuring the Au(111) Shockley surface state before all STS measurements. STS was performed under open feedback conditions by lock-in detection of the tunnel current driven by a wiggle voltage having a magnitude of 6–16 V rms at 401 Hz added to the tunneling bias. WSxM software was used to process all STM and AFM images.

Supporting Information

Supporting Information is available from the Wiley Online Library or from the author.

Acknowledgements

This work was supported by the U.S. Department of Energy, Office of Science, Office of Basic Energy Sciences, Materials Sciences and Engineering Division (DE-AC02-05-CH11231), within the Nanomachine program (KC1203 which provided for STM imaging, spectroscopy, and analysis). Support was also provided by the Molecular Foundry at LBNL funded by the U.S. Department of Energy, Office of Science, Office of Basic Energy

Sciences, Scientific User Facilities Division (DE-AC02-05CH11231), which provided for graphene device fabrication; by the National Science Foundation Award CHE-2204252 (molecular deposition and characterization); by the EPSRC grant EP/S025324/1 (calculation of molecular vdW bonding energy from DFT); by the Thomas Young Centre under grant number TYC-101 (Monte Carlo simulations); by the Imperial College London Research Computing Service (DOI: 10.14469/hpc/2232) (DFT calculation of molecular chain electronic structure); and by JSPS KAKENHI Grant Number 20H00354, 21H05233, and 23H02052 and World Premier International Research Center Initiative (WPI), MEXT, Japan. (growth of hBN crystals). F.L. acknowledges support from a Kavli Ensi Philomathia Graduate Student Fellowship. Z.G. was supported through a studentship in the Centre for Doctoral Training on Theory and Simulation of Materials at Imperial College London funded by the EPSRC (EP/L015579/1). We thank J.M. Kahl for useful discussions.

Conflict of Interest

The authors declare no conflict of interest.

Author Contributions

F.L. and H.-Z.T. contributed equally to this work. Conceptualization was done by F.L., H.-Z.T., A.A., and M.C.; Methodology was done by F.L., H.-Z.T., A.A., Z.G., and J.L.; Investigation was done by F.L., H.-Z.T., A.A., E.H., M.H., K.W., T.T., and M.C.; Visualization was done by F.L., H.-Z.T., A.A., and Y.Y.; Funding acquisition was done by J.L. and M.C.; Project administration was done by J.L. and M.C.; Supervision was done by J.L. and M.C.; Writing was done by F.L., H.-Z.T., Z.G., J.L., and M.C.; Review and editing were written by F.L., H.-Z.T., Z.G., J.L., and M.C.

Data Availability Statement

The data that support the findings of this study are available from the corresponding author upon reasonable request.

Keywords

field-driven phase transitions, graphene field-effect transistor, molecular solids, nonequilibrium dynamics, solid–liquid phase coexistence

Received: January 17, 2023

Revised: June 6, 2023

Published online:

- [1] H. Guo, K. Chen, Y. Oh, K. Wang, C. Dejoie, S. A. Syed Asif, O. L. Warren, Z. W. Shan, J. Wu, A. M. Minor, *Nano Lett.* **2011**, *11*, 3207.
- [2] K.-A. N. Duerloo, Y. Li, E. J. Reed, *Nat. Commun.* **2014**, *5*, 4214.
- [3] S. Song, D. H. Keum, S. Cho, D. Perello, Y. Kim, Y. H. Lee, *Nano Lett.* **2016**, *16*, 188.
- [4] W. Li, L. Kong, B. Feng, H. Fu, H. Li, X. C. Zeng, K. Wu, L. Chen, *Nat. Commun.* **2018**, *9*, 198.
- [5] C. Liu, S. Yamazaki, R. Hobara, I. Matsuda, S. Hasegawa, *Phys. Rev. B* **2005**, *71*, 041310.
- [6] K. F. Mak, J. Shan, D. C. Ralph, *Nat. Rev. Phys.* **2019**, *1*, 646.
- [7] H. Kuwahara, Y. Tomioka, A. Asamitsu, Y. Morimoto, Y. Tokura, *Science* **1995**, *270*, 961.
- [8] F. Zhang, H. Zhang, S. Krylyuk, C. A. Milligan, Y. Zhu, D. Y. Zemlyanov, L. A. Bendersky, B. P. Burton, A. V. Davydov, J. Appenzeller, *Nat. Mater.* **2019**, *18*, 55.
- [9] B. Wortmann, D. V. Vörden, P. Graf, R. Robles, P. Abufager, N. Lorente, C. A. Bobisch, R. Möller, *Nano Lett.* **2016**, *16*, 528.
- [10] J. Crossno, J. K. Shi, Ke Wang, X. Liu, A. Harzheim, A. Lucas, S. Sachdev, P. Kim, T. Taniguchi, K. Watanabe, T. A. Ohki, K. C. Fong, *Science* **2016**, *351*, 1058.
- [11] M. Kühne, F. Börrnert, S. Fecher, M. Ghorbani-Asl, J. Biskupek, D. Samuelis, A. V. Krashennnikov, U. Kaiser, J. H. Smet, *Nature* **2018**, *564*, 234.
- [12] T. Nakamuro, M. Sakakibara, H. Nada, K. Harano, E. Nakamura, *J. Am. Chem. Soc.* **2021**, *143*, 1763.
- [13] A. Alessandrini, P. Facci, *Soft Matter* **2014**, *10*, 7145.
- [14] F. Liou, H.-Z. Tsai, A. S. Aikawa, K. C. Natividad, E. Tang, E. Ha, A. Riss, K. Watanabe, T. Taniguchi, J. Lischner, A. Zettl, M. F. Crommie, *Nano Lett.* **2021**, *21*, 8770.
- [15] J.-P. Hansen, I. R. McDonald, in *Theory of Simple Liquids*, 3rd ed., Academic Press, Amsterdam, The Netherlands **2006**, pp. 46–77.
- [16] Y. Zhang, V. W. Brar, F. Wang, C. Girit, Y. Yayon, M. Panlasigui, A. Zettl, M. F. Crommie, *Nat. Phys.* **2008**, *4*, 627.
- [17] S. Wickenburg, J. Lu, J. Lischner, H.-Z. Tsai, A. A. Omrani, A. Riss, C. Karrasch, A. Bradley, H. S. Jung, R. Khajeh, D. Wong, K. Watanabe, T. Taniguchi, A. Zettl, A. H. C. Neto, S. G. Louie, M. F. Crommie, *Nat. Commun.* **2016**, *7*, 13553.
- [18] R. Decker, Y. Wang, V. W. Brar, W. Regan, H.-Z. Tsai, Q. Wu, W. Gannett, A. Zettl, M. F. Crommie, *Nano Lett.* **2011**, *11*, 2291.
- [19] D. A. Rehn, Y. Li, E. Pop, E. J. Reed, *npj Comput. Mater.* **2018**, *4*, 2.
- [20] A. H. Castro Neto, F. Guinea, N. M. R. Peres, K. S. Novoselov, A. K. Geim, *Rev. Mod. Phys.* **2009**, *81*, 109.
- [21] M. Kim, J. R. Chelikowsky, *Appl. Phys. Lett.* **2015**, *107*, 163109.

ADVANCED MATERIALS

Supporting Information

for *Adv. Mater.*, DOI 10.1002/adma.202300542

Imaging Field-Driven Melting of a Molecular Solid at the Atomic Scale

*Franklin Liou, Hsin-Zon Tsai, Zachary A. H. Goodwin, Andrew S. Aikawa, Ethan Ha, Michael Hu, Yiming Yang, Kenji Watanabe, Takashi Taniguchi, Alex Zettl, Johannes Lischner and Michael F. Crommie**

Supplementary Materials for

Imaging Field-Driven Melting of a Molecular Solid at the Atomic Scale

Authors: Franklin Liou^{1,2,3}, Hsin-Zon Tsai^{1,2}, Zachary A. H. Goodwin^{4,5,6}, Andrew S. Aikawa^{1,2}, Ethan Ha¹, Michael Hu¹, Yiming Yang¹, Kenji Watanabe⁷, Takashi Taniguchi⁸, Alex Zettl^{1,2,3}, Johannes Lischner⁴, and Michael F. Crommie^{1,2,3*}

Affiliations:

¹Department of Physics, University of California at Berkeley, Berkeley, CA 94720, United States.

²Materials Sciences Division, Lawrence Berkeley National Laboratory, Berkeley, CA 94720, United States.

³Kavli Energy NanoSciences Institute at the University of California at Berkeley, Berkeley, CA 94720, USA.

⁴Department of Materials, Imperial College London, Prince Consort Rd, London SW7 2BB, UK.

⁵National Graphene Institute, University of Manchester, Booth St. E. Manchester M13 9PL, United Kingdom

⁶School of Physics and Astronomy, University of Manchester, Oxford Road, Manchester M13 9PL, United Kingdom

⁷Research Center for Functional Materials, National Institute for Materials Science, 1-1 Namiki, Tsukuba 305-0044, Japan

⁸International Center for Materials Nanoarchitectonics, National Institute for Materials Science, 1-1 Namiki, Tsukuba 305-0044, Japan

[†]F.L. and H.-Z. T. contributed equally to this paper

*Corresponding author: crommie@berkeley.edu.

This PDF file includes:

Materials and Methods:	Page
(1) Resolving solid and liquid phase structures with STM	3
(2) Device capacitance measurement	4
(3) Determining E_F from V_G and N_I (analytical model)	4

(4) Determining N_l^{eq} from minimization of $U(N_l, E_F)$	5
(5) DFT calculations	6
(6) Monte Carlo simulations	9
(7) Radial distribution function calculation	12
(8) Structural characterization of molecular chains	13
(9) Long-term monitoring of phase equilibrium	17
(10) Thermodynamic theory of electrostatically-driven phase transitions in the grand potential framework	19

Figs. S1 to S10

Captions for Movies S1 to S3 (pages 20-21)

References (pages 21-22)

Other Supplementary Materials for this manuscript include the following:

Movies S1 to S3

Materials and Methods

(1) Resolving solid and liquid phase structures with STM

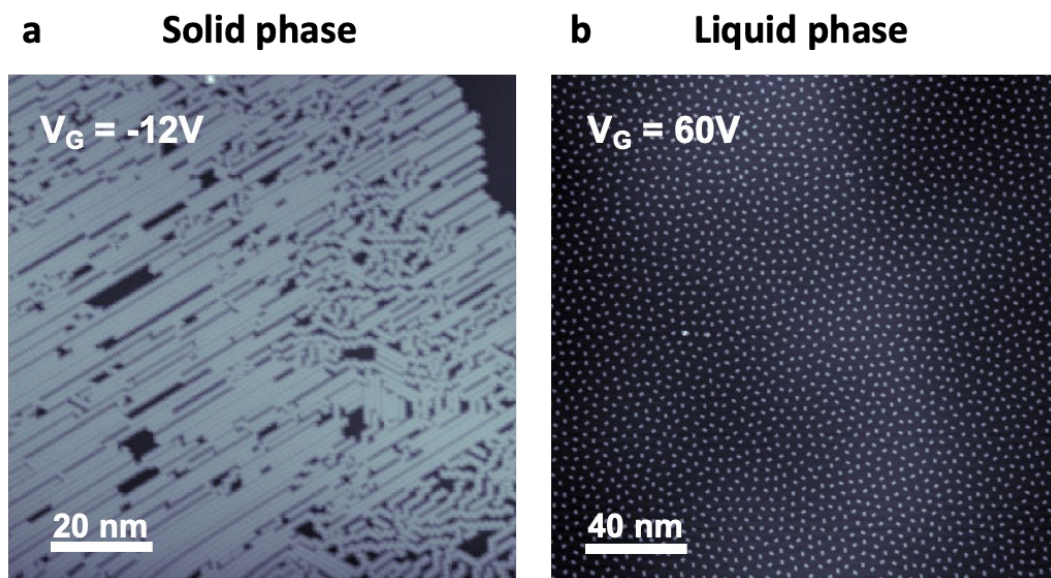


Fig. S1: Self-assembled F₄TCNQ structures on graphene in the solid and liquid phases. (a) An STM image of molecular chains (the “solid” phase) reveals two coexisting tiling geometries, linear and zig-zag, both with an intermolecular distance of 8.5 Å ($I = 1$ pA, $V = 2V$). This image was obtained after allowing the sample to reach equilibrium under diffusive conditions with $I_{SD} = 1.9$ mA and $V_G = -12V$. (b) Molecules in the ionic liquid phase show an evenly spaced distribution ($I = 1$ pA, $V = 2V$). This image was obtained after allowing the sample to reach equilibrium under diffusive conditions with $I_{SD} = 1.15$ mA and $V_G = 60V$. The structure factor $S(\mathbf{q})$ and radial distribution function $g(r)$ plotted in Fig. 1(k) of the main text are both extracted from the molecular positions shown in this image.

(2) Device capacitance measurement

The capacitance of our graphene device was determined by fitting the Dirac point energy as a function of gate voltage obtained from dI/dV spectra taken on pristine graphene. The method we used for fitting the Dirac point energy for each dI/dV curve is described in ref. [1]. We then used the following well-known expression to fit the energy position of the Dirac point as a function of applied gate voltage for a graphene FET:

$$E_D(V_G) = -\text{sgn}(V_G)\hbar v_F\sqrt{\pi C|V_G - V'|}, \quad (\text{S1})$$

where V' is a shift arising from impurity doping (which can vary with location). The extracted value of capacitance per area is $(6.9 \pm 0.1) \times 10^{10} |e| V^{-1} cm^{-2}$.

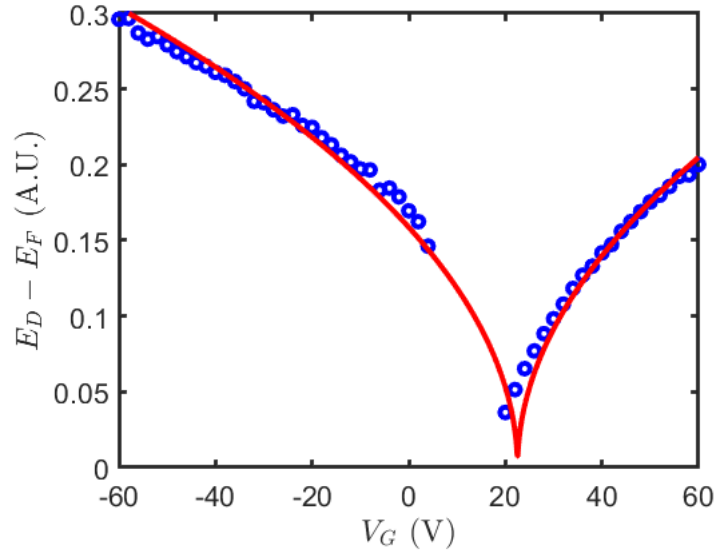


Fig.S2: Extracting device capacitance: The device capacitance of $6.9 \times 10^{10} |e| V^{-1} cm^{-2}$ was extracted by fitting Eq.(S1) (solid curve) to our FET data (circles).

(3) Determining E_F from V_G and N_l (analytical model)

To find E_F (the graphene FET Fermi energy) in terms of N_l (the total number of liquid phase molecules) and V_G (the backgate voltage) we make use of total charge conservation for

electrons in the molecular LUMO and graphene band states. Assuming no intrinsic charge doping on the pristine graphene device, the total charge density introduced by electrostatic gating the molecule-decorated device is $-CV_G$ (in units of $|e| \text{ cm}^{-2}$). Electrons introduced by gating can either occupy molecular LUMO states or graphene band states. Since each molecular LUMO can carry one electron of charge, the charge density carried by N_l isolated molecules over an area A is $\frac{-N_l}{A} |e| \text{ cm}^{-2}$. The charge density held in the graphene band states is given by the difference between the Fermi level E_F and the Dirac point energy E_D : $\frac{|E_D - E_F|^2}{\pi \hbar^2 v_F^2}$ ($E_F < E_D$ for the regime relevant this work). Combining these charge densities yields:

$$-CV_G = -\frac{N_l}{A} + \frac{|E_D - E_F|^2}{\pi \hbar^2 v_F^2}. \quad (\text{S2})$$

This expression allows us to express E_F as a function of N_l and V_G :

$$E_F = E_D - \sqrt{\pi \hbar^2 v_F^2 \left(\frac{N_l}{A} - CV_G \right)}. \quad (\text{S3})$$

(4) Determining N_l^{eq} from minimization of $U(N_l, E_F)$:

Starting from the expression for total energy U in Eq. (4) of the main text, we find that for N total molecules on the surface (with the number of liquid phase molecules $= N_l$), U can be expressed as

$$U = E_L N_l - \alpha(N - N_l - 1) + \frac{2A}{3\pi \hbar^2 v_F^2} [E_L^3 - E_F^3 + \frac{3}{2} E_D E_F^2 - \frac{3}{2} E_D E_L^2]. \quad (\text{S4})$$

Minimizing U with respect to N_l ,

$$\left. \frac{\partial U}{\partial N_l} \right|_{N_l = N_l^{eq}} = (E_L + \alpha) + \frac{2A(E_D - E_F)E_F}{\pi \hbar^2 v_F^2} \left. \frac{\partial E_F}{\partial N_l} \right|_{N_l = N_l^{eq}} = 0 \quad (\text{S5})$$

yields the equilibrium density of molecules N_l^{eq}/A expressed in Eq. (5) of the main text:

$$\frac{N_L^{eq}}{A} = CV_G + \frac{|E_D - (E_L + \alpha)|^2}{\pi \hbar^2 v_F^2} .$$

(5) DFT calculations

We performed *ab initio* DFT simulations of molecular chains in vacuum and also for a pair of molecules on graphene using the FHI-aims code^{2,3} with the PBE functional⁴ and a Hirshfeld van der Waals correction,⁵ as well as a tier 2 basis set for all atoms. These results show that DFT-calculated electronic structure of the molecular chains is consistent with the experimental results shown in the main manuscript, as follows:

(a) LUMO energies of chains:

In order to understand the chain electronic structure as a function of chain length, the molecules were arranged in zig-zag and linear chains and the atomic positions of molecular chains were allowed to relax until the forces on each atom became smaller than 0.005 eV/Ångstrom, while constraining the *z*-coordinates of all atoms to lie in a plane.

Fig. S3 shows the Kohn-Sham LUMO energies $E_L^{(N)}$ of chains with N molecules (up to $N = 8$) relative to the LUMO energy of an isolated molecule $E_L^{(1)}$, $\Delta E = E_L^{(N)} - E_L^{(1)}$. The LUMO energies of the chains are always higher than the LUMO energy of the isolated molecule and ΔE approaches approximately 40 meV as N increases. Plotting the wavefunctions of the chain end LUMO states (see Fig. S4) reveals that they are localized on the outermost molecules of the chain. The higher-lying unoccupied states of the chains are formed from the LUMOs of molecules in the middle of the chain. These levels lie approximately 80 meV higher than the single molecule LUMO for long chains. These results are in good agreement with the experimental findings.

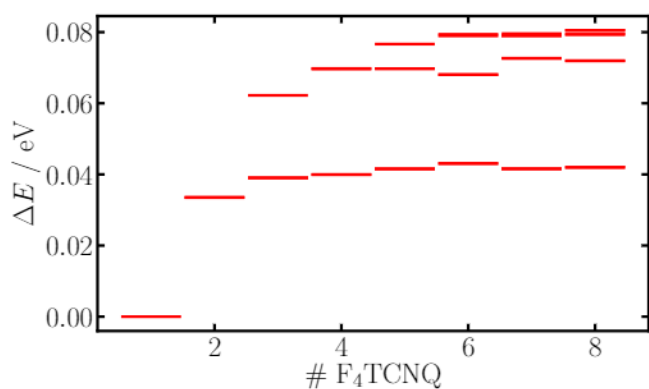


Fig. S3: F₄TCNQ LUMO energies, relative to that of the isolated molecule, obtained from DFT as a function of number of molecules in a molecular chain. An isolated molecule has the lowest LUMO energy, while molecules within a chain have higher LUMO energies, with the end molecules on the chain having a LUMO which is lower in energy than the rest of the molecules in the chain.

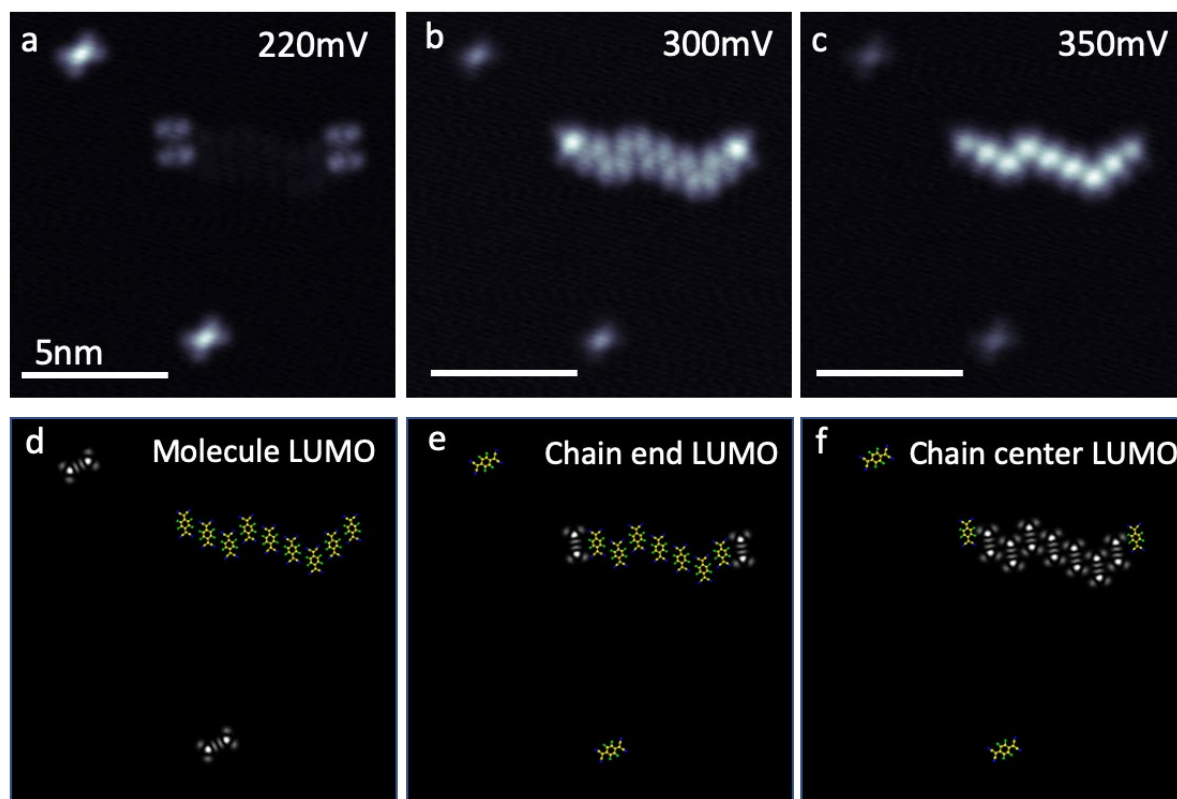


Fig. S4: dI/dV maps of F4TCNQ near LUMO energies of different molecular

configurations. (a)-(c) Experimental dI/dV maps of a chain and single molecules taken under an external gate voltage $V_G = -60\text{V}$ at different energies (for the same region of surface) (a) $V_s = 220\text{ mV}$, (b) $V_s = 300\text{ mV}$, (c) $V_s = 350\text{ mV}$. The dI/dV maps confirm that the single molecule LUMO is the lowest in energy, followed by molecules at the chain end, and then molecules at the center of the chain. (d)-(f) Theoretical electron density contour at energies corresponding to LUMOs of the single molecule, chain end, and chain center.

(b) Inter-molecule bonding energy (α):

To calculate the bonding energy between F4TCNQ molecules in a chain we prepared a graphene flake consisting of 8×8 graphene unit cells and hydrogen-passivated edges. The structure was relaxed while constraining the z-positions of the atoms to reside in a plane. We then performed constrained DFT calculations for a pair of adsorbed F4TCNQ molecules to ensure that the molecules remain uncharged (reflecting the uncharged character of molecules in chains), see Fig. S5. The binding energy was calculated from

$$-\alpha = E_{pair} - (E_{single,1} + E_{single,2} - E_{gra}), \quad (\text{S6})$$

where E_{pair} is the total energy of both molecules on the graphene flake, E_{gra} is the energy of the graphene flake without any molecules, and $E_{single,1/2}$ denotes the energy when one or the other molecule is removed from the flake. Note E_{gra} is needed to cancel the double counting of the energy of the flake from $E_{single,1} + E_{single,2}$. We find that the bonding energy is $\alpha \sim 45\text{ meV}$ from these calculations. This is similar to the experimental upper bound on α that was determined from our STM spectroscopy ($\alpha_{exp.} \lesssim 40\text{ meV}$).

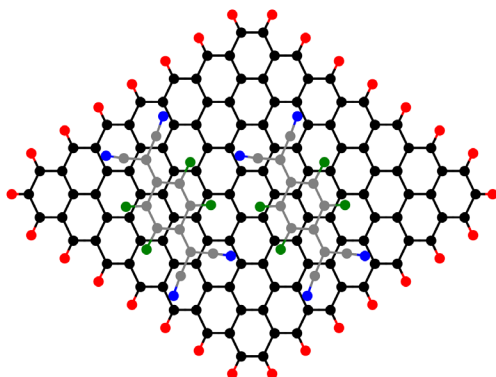


Fig. S5: Graphene flake with two adsorbed F4TCNQ molecules.

(6) Monte Carlo simulations

We employed a standard Metropolis Monte Carlo algorithm to simulate the dynamical collective behavior of uncharged molecules in chains together with isolated molecules (both charged and uncharged), and electrons residing in either the LUMO of isolated molecules or in graphene Dirac band states. The thermal energy in the simulations was taken to be $k_B T = 1$ meV.

For our simulations the molecules occupy sites on a coarse-grained triangular lattice with an area per site corresponding to 12 graphene unit cells and a lattice spacing of approximately 1 nm, see Fig. S6. A molecule can have one of three possible orientations which point along the vectors connecting a graphene carbon atom to nearest neighbor sites. This lattice is constructed as follows: if a molecule occupies a given site, the neighboring sites (shown in green in the top left panel of Fig. S6) are the ones that the nearest-neighbor molecules would occupy if the molecules were part of the same chain (either zigzag or linear). The red sites in the top left panel of Fig. S6 are nearest-neighbor sites that cannot be occupied because we only consider side-by-

side bonding and not end-to-end bonding of molecules (since the latter is not observed experimentally). If a second molecule occupies one of the two neighboring sites on one “side” of the first molecule, then the other site becomes inaccessible (see top right panel of Fig. S6). As a consequence, each molecule can only form up to two bonds with its neighbors. A third molecule can occupy one of two sites on the other “side” of the first molecule which gives rise to either a zigzag arrangement (bottom left panel) or a linear configuration (bottom right panel). The energy per bond is taken to be -10 meV.

Electrons can either occupy graphene states or the LUMO of isolated molecules (we ignore the possibility of charged chains, but allow for uncharged isolated molecules). If a molecule becomes charged, it induces an electrostatic Hartree potential which is experienced by the other charged molecules. The corresponding contribution to the total energy is given by

$$E_H = \frac{1}{2} \sum_{i \neq j} W_{ij} n_i n_j, \quad (S7)$$

where $n_{i/j}$ are the charges of the molecules ($-|e|$ or 0), i and j label the isolated molecules located at positions $\boldsymbol{\tau}_{i/j}$, and W_{ij} is the screened Coulomb interaction between these charges. In our simulations, we use the Thomas-Fermi theory result for doped graphene, i.e. $W_{ij} = e^2 / (4\pi\epsilon_0\epsilon\kappa^2 |\boldsymbol{\tau}_j - \boldsymbol{\tau}_i|^3)$ with κ denoting the inverse screening length and ϵ the background dielectric constant. We use $1/(\epsilon\kappa^2) = 25$. In this context the molecules are treated as point charges located on the sites of the effective triangular lattice.

At the beginning of the simulation 300 molecules are distributed randomly on a 50x50 supercell of the effective triangular lattice. The molecular orientations are also initially random. Next, we generate a trial move which is either accepted or rejected by the Monte Carlo algorithm and one iteration of the algorithm is completed when each of the 300 molecules has carried out a trial move. In each move, the molecules can hop from their current site to nearest neighbor sites

and also change orientation. We consider three cases: (i) if an isolated molecule hops onto the nearest neighbor site of another molecule, its orientation aligns with that of its neighbor and a bond is formed; (ii) if an isolated molecule hops onto a site without nearest neighbors, its orientation changes randomly; (iii) if a molecule dissociates from a chain, its orientation does not change.

To generate a more realistic initial configuration corresponding to the experimental setup, we performed 160 iterations in the presence of a linear potential in the x-direction with a gradient of -10 meV/nm to mimic the electromigration force of the flowing current used experimentally to create initial molecular configurations. Then 150 electrons were added into graphene states (assuming that all graphene states up to the molecular LUMO level are always filled) and turned off the electromigration potential. In the presence of the electrons, the procedure for a single move in the Monte Carlo simulation was extended according to the following rules: (i) if a molecule is uncharged and not bound to another molecule after it has hopped to a nearest-neighbor site, an electron can be transferred from the highest occupied graphene state to the LUMO; (ii) if an isolated molecule is initially charged and does not form a bond to another molecule in the move, its charge can be transferred to the graphene; (iii) if a molecule is converted from an isolated, uncharged state to a bonded configuration, it cannot become charged in that move; (iv) if a molecule is initially charged and forms a bond to another molecule, its charge must be transferred to the graphene; (v) if a molecule dissociates from a chain, it can become charged.

After each extended move involving a molecular displacement, re-orientation, electron transfer, or bond formation, the change in the total energy of the system (now consisting of a term describing the electrons in the graphene, a term describing the bonding between molecules,

a term describing the charging of molecules, and the Hartree interaction between charged molecules) is calculated and the Monte Carlo algorithm decides whether to reject or accept the move. We ran the simulation for 400 iterations.

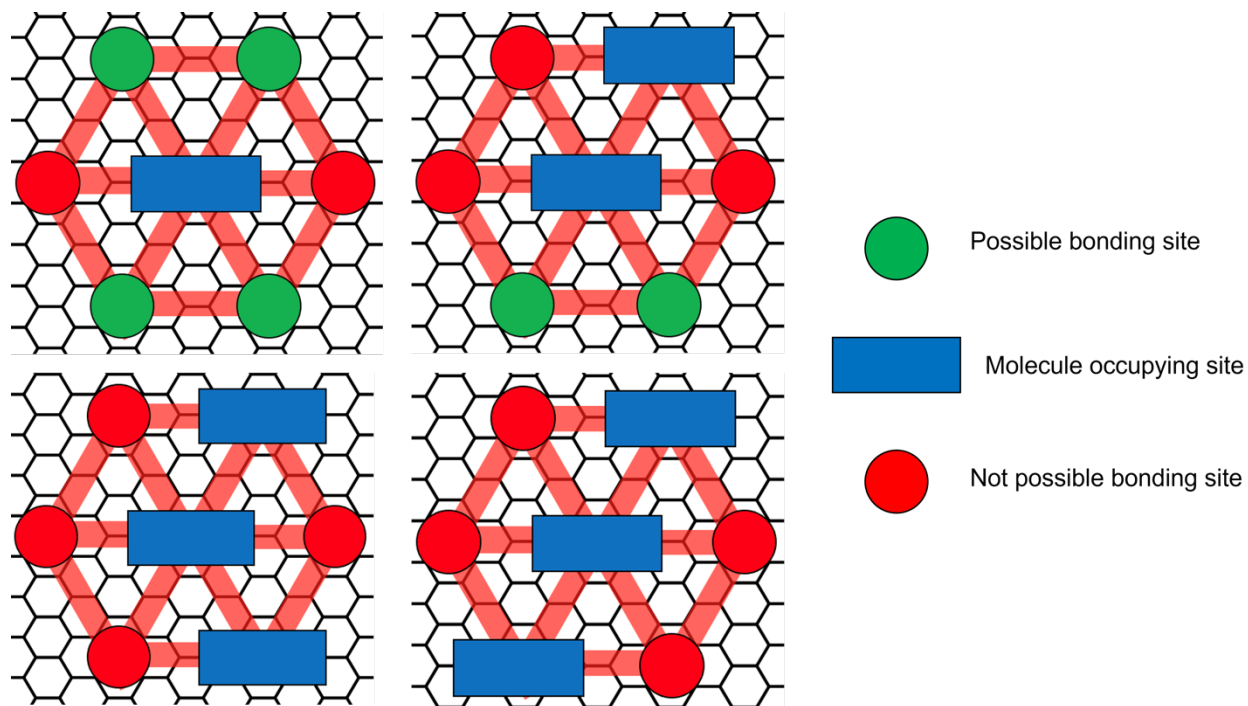


Fig. S6: Allowed adsorption sites defined in the Monte Carlo simulation: The allowed adsorption sites form a triangular lattice. Adsorbed molecules can either form a zigzag chain (bottom left) or a linear chain (bottom right).

(7) Radial distribution function calculation

After obtaining the molecular centroid positions r_i using the trackpy software suite,⁶ the radial distribution function $g(r)$ shown in Fig. 1(k) of the main text was calculated using this standard definition:⁷

$$g(r) = \frac{1}{\rho_{avg}} \left\langle \frac{dN_i(r)}{2\pi r dr} \right\rangle \quad (S8)$$

where $N_i(r)$ is the number of molecules within a concentric ring of radius r and thickness dr centered around molecule i , and ρ_{avg} is the average density of molecules on the surface.

Molecules within the radial bin $(r, r + dr)$ contribute to the count of $N_i(r)$. The ensemble average $\langle \cdot \rangle$ is then taken over all molecules i within a radius of $r \leq d/4$ of the center of the scan frame, where d is the width of the square scan frame (this is to ensure exclusion of edge molecules so that the average is not skewed by edge effects).

(8) Structural characterization of molecular chains

The structure factor, $S(\mathbf{q})$, of the solid chain phase was determined by first recording the center positions of molecules within linear and zigzag chains using STM topography (Figs. S7(a), (c)). $S(\mathbf{q})$ was then obtained from the molecular positions using the freud-analysis numerical analysis software.⁸ (Figs. S7(b), (d)). The structure factor $S(\mathbf{q})$ is defined as

$$S(\mathbf{q}) = \frac{1}{N} \sum_{j=1}^N \sum_{k=1}^N e^{-i\mathbf{q} \cdot (\mathbf{R}_j - \mathbf{R}_k)} \quad (S9)$$

where \mathbf{R}_j , \mathbf{R}_k are the centroid positions of pairs of molecules, and the sum is taken over all N particles. The molecular quasi-1D solid chain geometries exhibit an $S(\mathbf{q})$ with a clear periodicity of $\sim (8.5\text{\AA})^{-1}$ along the chain growth direction (Fig. S7 (a), (b)). In the direction perpendicular to the chain growth, the periodicity is less well-defined due to variability in inter-chain separation, thus corroborating that the molecules are in a quasi-1D solid. Molecules self-assembled into a mixture of zigzag and linear chain geometries (Fig. S7(c)) exhibit an $S(\mathbf{q})$ that shows an array of diffraction spots separated by $\sim (8.5\text{\AA})^{-1}$ (Fig. S7(d)). In the direction perpendicular to the chain

growth, however, the periodicity is again less well-defined due to the variability in inter-chain distance, corroborating the quasi-1D structure. We found that the inter-molecular distance within a molecular chain is partially constrained by the underlying graphene lattice. In Fig. S8 we show STM topography data indicating that molecular chains are aligned with the underlying graphene lattice (the graphene lattice orientation was found from atomically-resolved STM topography data). The adsorption sites of molecules within chains are observed to lie on the “bridge” site of graphene (i.e., the center point of the molecule). The resulting inter-molecule separation within molecular chains is 8.52Å. In Fig. S9 dI/dV spectroscopy data is shown that was taken on different molecules within two molecular chains. Molecules 1 and 2 are part of a linear chain segment in the first chain and molecules 3, 4, 5 are part of a zigzag chain segment. The LUMO energies of the molecules within both the linear and zigzag segments are found to be nearly identical.

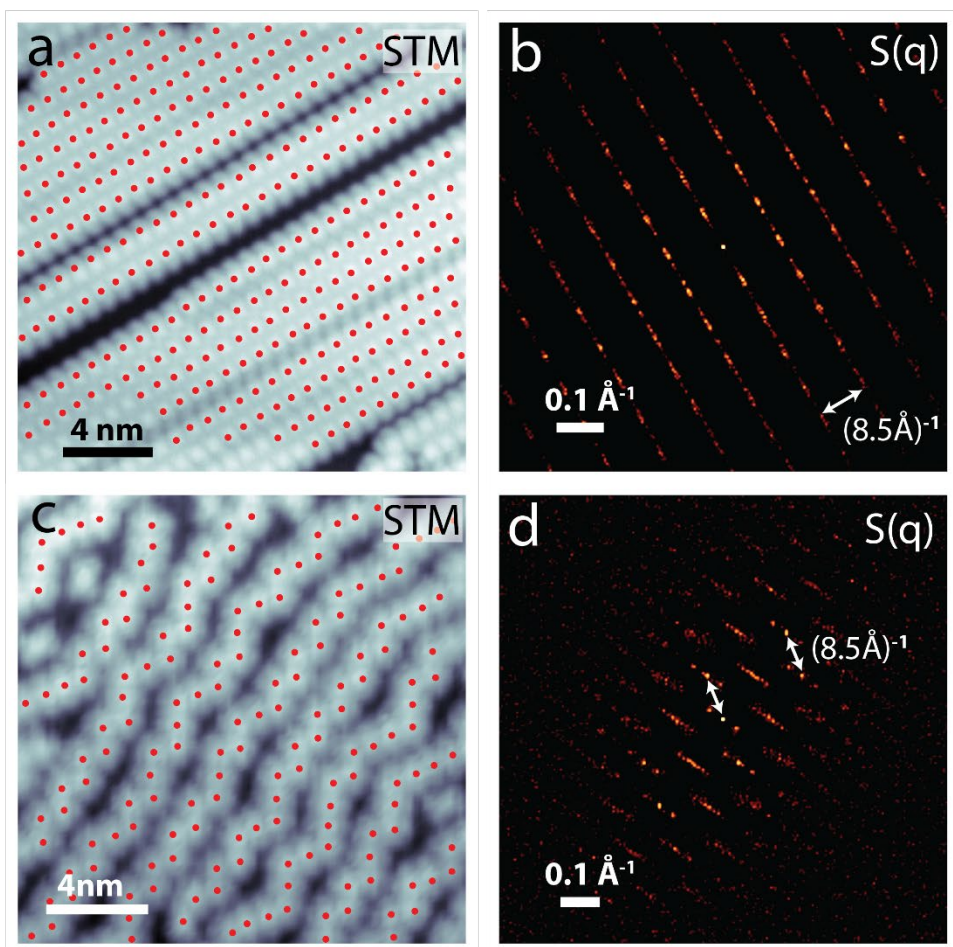


Fig. S7: Structural characterization of different molecular chain geometries: (a) STM topography of molecular chains in the linear geometry. Red dots indicate the center positions of the identified molecules. (b) The corresponding structure factor $S(\mathbf{q})$ calculated from the molecule center positions found in (a). (c) STM topography of molecular chains of mixed zigzag and linear geometries. (d) The corresponding structure factor $S(\mathbf{q})$ calculated from the molecule center positions found in (c).

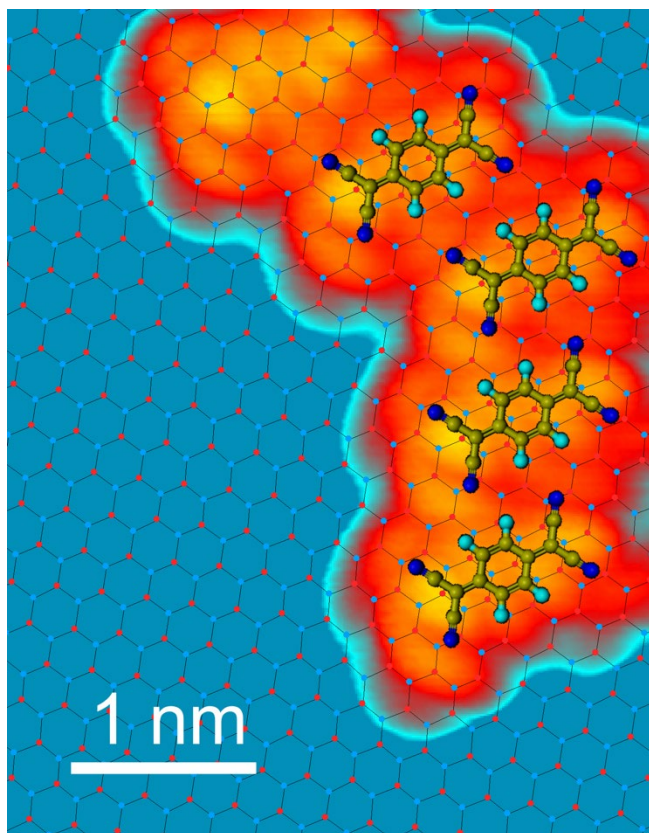


Fig. S8: Structure of molecular chains overlaid on the graphene lattice: STM topography of a molecular chain (including molecular model) overlaid on top of the measured graphene lattice. The graphene lattice orientation was found from atomically-resolved STM topography data. The inter-molecular distance of molecular chains was found to be 8.52\AA .

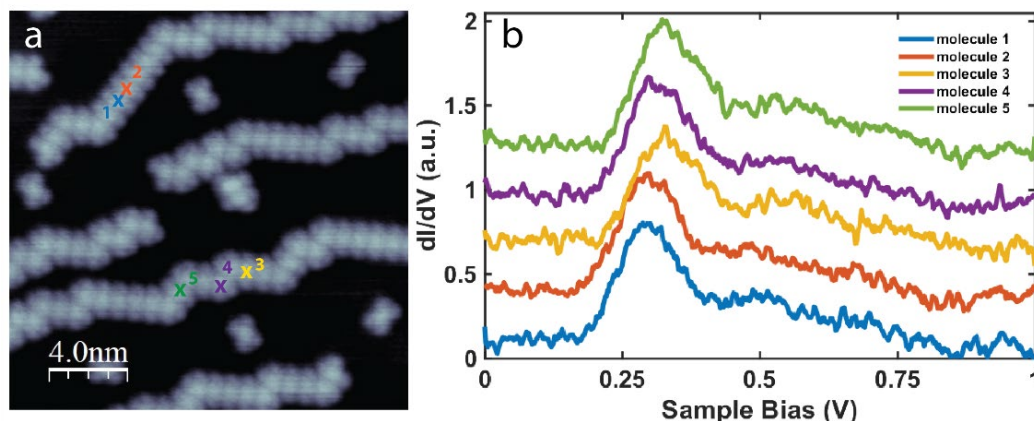


Fig. S9: dI/dV spectra of molecules in different structural geometries within molecular chains: (a) STM topography of molecular chains. (b) dI/dV spectra taken on different molecules located at positions marked by an “x” in (a).

(9) Long-term monitoring of phase equilibrium:

In order to determine the sufficient current and pulse duration to reach equilibrium between solid and liquid phase molecules, we performed long-term monitoring of the solid-liquid phase boundary under different current pulse durations. This can be seen in Fig. S10 which shows an experiment where a source-drain current of 1mA was used to heat the device while the gate voltage V_G was held at -20V. The surface molecular configuration was initially prepared by heating the device with 1mA current at $V_G = -60V$ for $\Delta t > 1$ sec. The resulting initial equilibrium surface molecular configuration is shown in Fig. S10 (a) and shows only solid-phase molecules as expected. The gate voltage was then switched to $V_G = -20V$ and source-drain current pulses of 1mA with durations ranging from 1, 20, 60, 180, and 600s were applied to the device. The resulting surface molecular configurations after the current pulses are shown in Fig. S10 (b)-(f).

We observe that the average concentration of molecules does not change significantly between 1s and 860s of current flow, thus demonstrating that equilibrium is reached within 1s of current pulse. We conclude that the pulse durations of 180s used in Fig. 1 (a)-(h) are sufficient to establish equilibrium between solid and liquid phases.

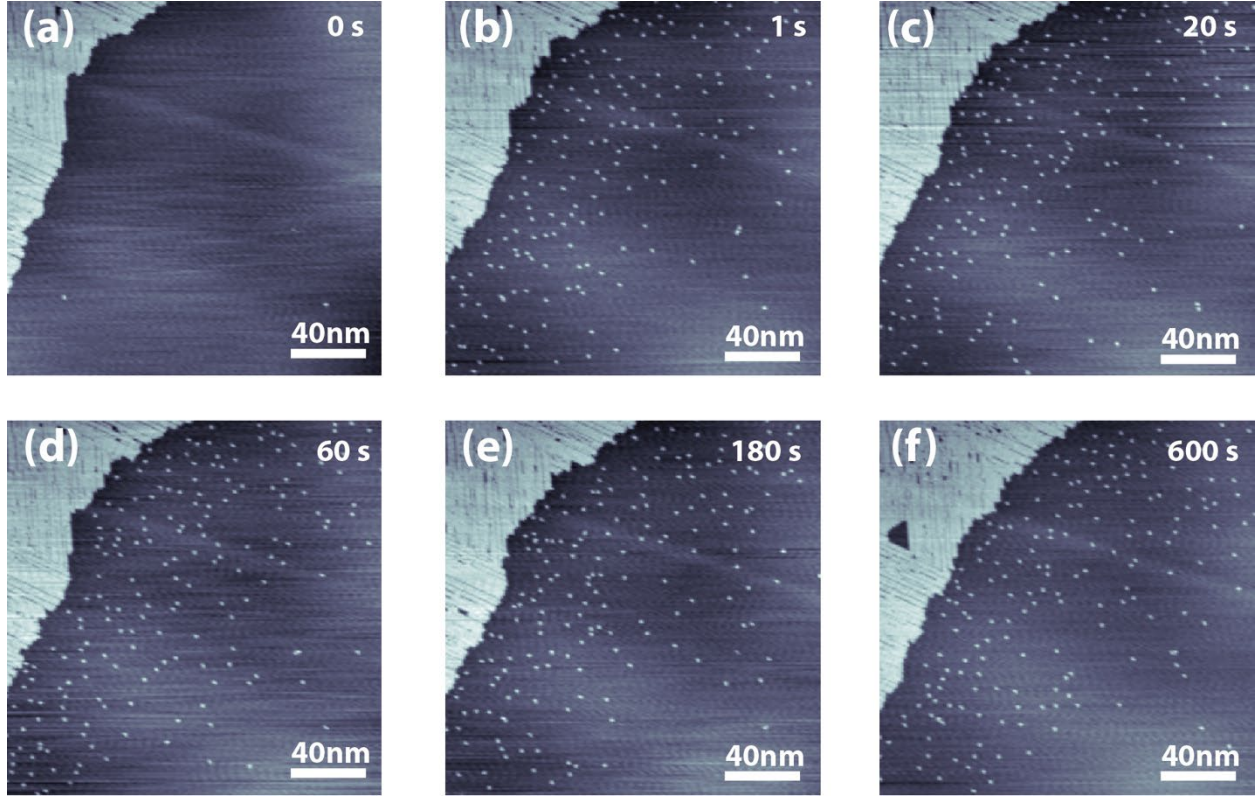


Fig. S10: Long-term stability of liquid- and solid-phase equilibrium: (a) STM topograph of the surface molecular configuration prepared by heating the graphene device with a 1mA source-drain current pulse for $\Delta t > 1$ sec while holding $V_G = -60V$. Solid phase molecules aggregate in the top left corner of the image. (b)-(f) STM topographs of the surface after applying a 1mA current pulse while holding $V_G = -20V$ for 1, 20, 60, 180, and 600s, respectively. The equilibrium densities of solid and liquid phase molecules is established within 1s of applying the current pulse while holding $V_g = -20V$.

(10) Thermodynamic theory of electrostatically-driven phase transitions in the grand potential framework

In an open system where particles are allowed to be exchanged with a reservoir, the thermodynamic potential that is minimized is the grand potential Φ . Since electrons can be moved between the silicon back gate (the reservoir) and the molecule-decorated graphene system by application of a gate voltage, the system is open for electrons. For all other particles, such as the solid phase molecules and liquid phase molecules, the system is closed, thus we define the grand potential to be

$$\Phi = U - TS - E_F N_e, \quad (\text{S6})$$

Where U is the internal energy of the system (graphene plus molecules), T is the overall temperature, S is the entropy of the system, E_F is the electrochemical potential of electrons (Fermi level) in the systems and N_e is the number of electrons in the system. Additionally, we can define a chemical potential μ_l and μ_s for the two other species of particles: liquid phase molecules and solid phase molecules, given N_l as the number of liquid phase molecules, and N_s as the number of solid phase molecules. The thermodynamic identity of this system then reads

$$d\Phi = -SdT - pdV - N_e dE_F + \mu_l dN_l + \mu_s dN_s. \quad (\text{S7})$$

Here the parallel between the Fermi level E_F and temperature T becomes clear: they both act as the natural variable (differential) term in the grand potential. If a temperature-driven first-order phase transition occurs, then the entropy of the two phases is discontinuous, resulting in a jump in the entropy between the two phases $\Delta S = \frac{d\Phi_l}{dT} \big|_{V, E_F, N_l=N, N_s=0} - \frac{d\Phi_s}{dT} \big|_{V, E_F, N_l=0, N_s=N}$, where Φ_l is the grand potential when all molecules are in the liquid phase, Φ_s is the grand potential when all molecules are in the solid phase, N is the total number of molecules, N_l is the number of liquid

phase molecules, and N_s is the number of solid phase molecules. The latent heat $T\Delta S$ is needed to melt all the solid phase molecules into liquid phase molecules for this first order phase transition. In analogy to this, for the case of an electrostatically-driven phase transition, the number of electrons in the system is the discontinuous quantity where $\Delta N_e = \frac{d\Phi_l}{dE_F} \big|_{V,T,N_l=N,N_s=0} - \frac{d\Phi_s}{dE_F} \big|_{V,T,N_l=0,N_s=N}$. The latent energy $E_F\Delta N_e$ is then needed to melt all the solid phase molecules into liquid phase molecules for this first order phase transition.

Movie access: Three movies showing solid-liquid phase transitions for F₄TCNQ molecules on graphene FET devices (Movie S1, Movie S2, and Movie S3) can be found at this website:

https://crommie.berkeley.edu/f4tcnq_movies

Movie Descriptions:

Movie S1: Molecules condensing into molecular chains: This movie shows sequential STM images of the surface configuration of F₄TCNQ molecules on graphene transforming from a liquid phase to a solid phase (i.e., a freezing transition). At the start of the movie, an equilibrium molecular configuration is shown that was prepared by simultaneously applying $I_{SD}=1.3\text{mA}$ and $V_G=60\text{V}$ to the graphene device for 180s. Each subsequent frame shows the sample after lowering V_G to $V_G=-5\text{V}$ and sending a current pulse through the device for $\Delta t=100\text{ms}$ (i.e., each frame shows a forward step in time of $\Delta t=100\text{ms}$ while keeping $V_G=-5\text{V}$ constant). Molecular chains are observed to continually condense throughout the movie.

Movie S2: Molecular chains dissociating into single molecules: This movie shows sequential STM images of the F₄TCNQ molecular configuration on graphene transforming from a solid

phase back to a liquid phase (i.e., a melting transition). This movie begins where Movie S1 ends, with the surface in a solid molecular configuration (i.e., “frozen”) that is obtained after holding the gate voltage at $V_G = -5$ V under diffusive conditions for $\Delta t = 500$ ms. In this movie V_G is set to $V_G = 60$ V and each frame shows the surface evolution after an amount of time $\Delta t = 500$ μ s while keeping the source-drain current at $I_{SD} = 1.1$ mA. Molecules are observed to dissociate from the chains (i.e., to melt) throughout the movie. By the end of this movie the surface molecular configuration has returned to the equilibrium configuration at $V_G = 60$ V seen at the beginning of Movie S1.

Movie S3: Wave of single molecules emerging from molecular chains: This movie shows sequential STM images of a highly nonequilibrium “wave” of liquid phase F₄TCNQ molecules on graphene emerging from a molecular solid. At the start of the movie an equilibrium molecular configuration is shown that was prepared by simultaneously applying $I_{SD} = 1$ mA and $V_G = -20$ V to the graphene device for 180 s. During the movie V_G is set to 60 V and each frame shows the time evolution of the surface after subjecting it to a source drain current of $I_{SD} = 1.3$ mA for $\Delta t = 100$ μ s. This is a nonequilibrium melting process.

References:

1. Liou, F. *et al.* Imaging Reconfigurable Molecular Concentration on a Graphene Field-Effect Transistor. *Nano Letters* **21**, 8770–8776 (2021).
2. Blum, V. *et al.* Ab initio molecular simulations with numeric atom-centered orbitals. *Computer Physics Communications* **180**, 2175–2196 (2009).

3. V. Blum *et al.* FHI-aims. All-electron electronic structure theory with numeric atom-centered orbitals. (2009).
4. Perdew, J. P., Burke, K. & Ernzerhof, M. Generalized Gradient Approximation Made Simple. *Physical Review Letters* **77**, 3865–3868 (1996).
5. Tkatchenko, A. & Scheffler, M. Accurate Molecular Van Der Waals Interactions from Ground-State Electron Density and Free-Atom Reference Data. *Physical Review Letters* **102**, 73005 (2009).
6. Allan, D. B., Caswell, T., Keim, N. C., van der Wel, C. M. & Verweij, R. W. soft-matter/trackpy: Trackpy v0.5.0. (2021) doi:10.5281/ZENODO.4682814.
7. Hansen, J.-P. & McDonald, I. R. Statistical Mechanics and Molecular Distribution Functions. in *Theory of Simple Liquids (Second Edition)* (eds. HANSEN, J. P. & McDONALD, I. A. N. R.) 13–44 (Academic Press, 1986). doi:<https://doi.org/10.1016/B978-0-08-057101-0.50006-8>.
8. Ramasubramani, V. *et al.* freud: A Software Suite for High Throughput Analysis of Particle Simulation Data. *Computer Physics Communications* **254**, 107275 (2020).